

OPEN

Transferred monolayer MoS₂ onto GaN for heterostructure photoanode: Toward stable and efficient photoelectrochemical water splitting

Mostafa Afifi Hassan¹, Min-Woo Kim², Muhammad Ali Johar¹, Aadil Waseem¹, Min-Ki Kwon² & Sang-Wan Ryu^{1,3*}

Solar-driven photoelectrochemical water splitting (PEC-WS) using semiconductor photoelectrodes is considered a promising solution for sustainable, renewable, clean, safe and alternative energy sources such as hydrogen. Here, we report the synthesis and characterization of a novel heterostructure MoS₂/GaN to be used as a photoanode for PEC-WS. The heterostructure was synthesized by metal-organic chemical vapor deposition of single crystalline GaN onto a c-plane sapphire substrate, followed by the deposition of a visible light responding MoS₂ monolayer ($E_g = 1.9$ eV) formed by a Mo-sulfurization technique. Our experimental results reveal that MoS₂/GaN photoanode achieved efficient light harvesting with photocurrent density of 5.2 mA cm⁻² at 0V vs Ag/AgCl, which is 2.6 times higher than pristine GaN. Interestingly, MoS₂/GaN exhibited a significantly enhanced applied-bias-photon-to-current conversion efficiency of 0.91%, whereas reference GaN yielded an efficiency of 0.32%. The superior PEC performance of the MoS₂/GaN photoelectrode is mainly related to the enhanced light absorption due to excellent photocatalytic behavior of MoS₂, which reduces charge transfer resistance between the semiconductor and electrolyte interface, and the improvement of charge separation and transport. This result gives a new perspective on the importance of MoS₂ as a cocatalyst coated onto GaN to synthesize photoelectrodes for efficient solar energy conversion devices.

With the concern of a global energy crisis and subsequent desire for alternative fuel sources, hydrogen (H₂) has drawn considerable interest as a future energy carrier since it is a clean fuel that produces no harmful byproducts after combustion^{1,2}. H₂, in particular, is one of the most promising energy carriers and fuel sources due to its high energy-per-mass content, wide range of available storage and transport approaches, and reduced harmful emissions^{3,4}. Indeed, the energy stored into its chemical bond can be used in fuel cells to produce clean electricity. One of the most promising solutions is represented by the use of photoelectrochemical cells (PECs) for light-driven water splitting. PEC water splitting using solar energy has attracted considerable attention in both scientific and industrial communities⁵. Because the fabrication process is simple and environmentally friendly, it has been considered one of the most attractive ways to produce H₂⁶. After it was firstly demonstrated by Fujishima and Honda in 1972 using TiO₂ to split water into H₂ and O₂, researchers have been studying candidates of high performance photoelectrode for PEC water splitting⁷⁻⁹. To achieve high energy conversion efficiency, photoanodes should effectively harvest the sunlight and facilitate charge transfer while they should exhibit long-term stability¹⁰. The conversion efficiency of solar energy to chemical energy in hydrogen molecule and the stability during PEC process are crucial features of PEC cells, which are mainly determined by the semiconducting material properties of the photoelectrodes^{11,12}. Therefore, many semiconductor materials including transition metal oxides have been explored primarily for PEC cells, such as TiO₂¹³, ZnO¹⁴, BiVO₄¹⁵, α -Fe₂O₃¹⁶ and WO₃¹⁷ due to the chemical stability, low cost, and easy fabrication¹⁸. However, they generally have wide band gaps and absorb a limited

¹Department of Physics, Chonnam National University, Gwangju, 61186, Republic of Korea. ²Department of Photonic Engineering, Chosun University, Gwangju, 61452, Republic of Korea. ³Optoelectronics Convergence Research Center, Chonnam National University, Gwangju, 61186, Republic of Korea. *email: sangwan@chonnam.ac.kr

portion of the solar spectrum, resulting in poor conversion efficiencies¹⁹. In pursuit of high-efficiency photoelectrodes for solar energy conversion applications, several crucial requirements should be satisfied, such as a suitable band gap value and appropriate band alignment of the working electrode with the water redox levels²⁰. In recent decades, tremendous efforts have been devoted toward exploring novel and efficient photoelectrode materials to improve the solar energy photoconversion efficiency. In order to gain desired solar-to-hydrogen conversion efficiency, heterojunction structures are desirable and considered as an important strategy because they allow for the combination of properties from each element, leading to an improved overall efficiency²¹. The fabricated heterojunction not only can expand the spectral range for light-absorption, but also can promote photoexcited electron–hole separation, which can minimize electron–hole recombination, thus significantly enhancing the energy efficiency²².

Recently, researchers have studied III-nitride based materials as potential candidates for PEC water-splitting and the generation of hydrogen energy due to their tunable bandgap, which spans nearly the entire solar spectrum, and a band-edge potential that meets the required water redox potentials^{23,24}. Among such III-nitride semiconductor materials used for achieving a desirable solar-to-hydrogen conversion efficiency, GaN has been intensively investigated due to its amazing intrinsic properties and nanotechnological importance. GaN has straddling band-edge positions with the redox potentials of water, which is a prerequisite for efficient charge transfer between a semiconductor and water-based electrolyte¹⁹. Its wide band gap can be tuned from ultraviolet to near infrared by forming alloy mixture with AlN and InN, which is useful for improving optical and structural properties²⁵. In addition, GaN is an inexpensive, non-toxic material with excellent chemical stability against harsh PEC process²⁶. As a result of the advantages mentioned above, GaN-based photoanodes have attracted scientists' attention as a competitive material for harvesting solar energy. However, a desired configuration of a highly efficient and reliable solar hydrogen generation system is still limited due to the disadvantages of the current status of GaN based photoanodes. Thus, several requirements should be satisfied such as a reliable and stable photoanode against photocorrosion and enhanced conversion efficiencies. The use of heterojunction structures or nanostructured cocatalysts with GaN photoanodes is an important strategy to achieve improved PEC performance²⁷. The cocatalyst roles not only can protect the photoanode against corrosion, but also may reduce the carrier recombination loss, thus significantly increasing the efficiency of the water splitting process. For instance, the deposition of NiO cocatalyst on GaN reported by our group was a good technique to inhibit surface corrosion by mitigating hole accumulation at the GaN/electrolyte surface^{28,29}.

Recently, two-dimensional (2D) transition-metal-dichalcogenides (TMDCs) have intrigued physicists and material scientists due to their distinctive optical and electrical properties, which can be beneficial for numerous devices and applications^{30–32}. Among various 2D TMDCs, the molybdenum disulfide (MoS₂) is especially attractive because of its tunable optical band gap, high chemical stability, earth abundance, nontoxicity, and low cost in comparison with noble metals^{33,34}. In-plane closely packed hexagonal arrangements of S–Mo–S atoms with covalent bonds compose two dimensional MoS₂ structure³⁵. These layers are held together by relatively weak van der Waals forces, which provide an advantage for exfoliating MoS₂ film into monolayers³⁶. Intrinsic MoS₂ offers n-type semiconducting properties, with a tunable band gap ($E_g = 1.2\text{--}1.9\text{ eV}$) that is classified by the number of layers³⁷. Bulk MoS₂ has an indirect band gap of $E_g = 1.2\text{ eV}$, while monolayer MoS₂ (ML-MoS₂) has a direct band gap of $E_g = 1.9\text{ eV}$ ^{37,38}, which suggests promise for application in PEC hydrogen generation³⁹. Very recently, ML-MoS₂ was considered as an important catalyst for both photocatalytic and electrocatalytic H₂ evolution reactions due to the existence of abundant exposed edges, with active sites stemming from the sulfur edges of the MoS₂ crystal layers^{40,41}. Moreover, MoS₂ thin films or nanosheets have been deposited onto ZnO NWs as cocatalysts, which suppressed the photocorrosion and increased the photocurrent densities⁴². Yong-Jun *et al.* reported that the intimate and large contact interface between MoS₂ and TiO₂ can efficiently promote photoinduced charge carrier separation, which leads to an extension of the charge carrier lifetime against recombination⁴³.

Herein, we report the synthesis and characterization of patterned highly crystalline ML-MoS₂ on GaN by a Mo-sulfurization technique. We also demonstrated application of the MoS₂/GaN heterostructure as a photoanode for PEC water splitting and proposed a mechanism for the process. The PEC characteristics are investigated in detail to evaluate the water splitting behavior of the heterostructure. In addition, improved PEC water splitting performance of the transferred ML-MoS₂ onto GaN photoanode enabled by the photocatalytic behavior of ML-MoS₂ is studied. The outcome of the study is that the MoS₂/GaN photoanode shows a better enhanced PEC performance than pristine GaN. Therefore, the present study can be useful for the development of heterostructure based photoanodes in PEC applications.

Results and Discussion

A schematic diagram of the MoS₂ synthesis procedure and the fabrication of MoS₂/GaN heterostructure photoanode is displayed in Fig. 1. Initially, a clean 2-inch sapphire substrate was patterned by photolithography to form square lattice patterns. A 1 nm-thick film of Mo was deposited on the sapphire substrate by using e-beam evaporation. The patterned Mo thin films were sulfurized into MoS₂ in a furnace, then the MoS₂ film was transferred to GaN on sapphire. Figure 2(a,b) shows the optical microscope images of the monolayer MoS₂ (ML-MoS₂) before and after the transfer process placed onto the sapphire and GaN substrates, respectively. It can be seen that the ML-MoS₂ maintains the same morphology after transfer. It is observed that this transfer technique does not introduce any cracks in the sample which suggests a clean surface and high-quality for the as-transferred samples. Patterned substrates with a uniform distribution of rectangular ML-MoS₂ (approximately $190 \times 110\ \mu\text{m}^2$ in size and $50\ \mu\text{m}$ apart) were obtained. Further systematic characterizations of the synthesized ML-MoS₂ were conducted with Raman spectroscopy and photoluminescence (PL) measurements. Raman spectroscopy is a common tool for determining the precise number of layers in MoS₂ films such as tri, bi, and ML-MoS₂. The Raman spectra for these MoS₂ films contain peaks due to the E_{2g}^1 and A_g^1 phonon modes. The spectra displayed in Fig. 2(c) showed two typical Raman modes for the as-synthesized MoS₂, E_{2g}^1 at $382.71\ \text{cm}^{-1}$ and A_g^1 at $402.61\ \text{cm}^{-1}$ ^{44,45}. The

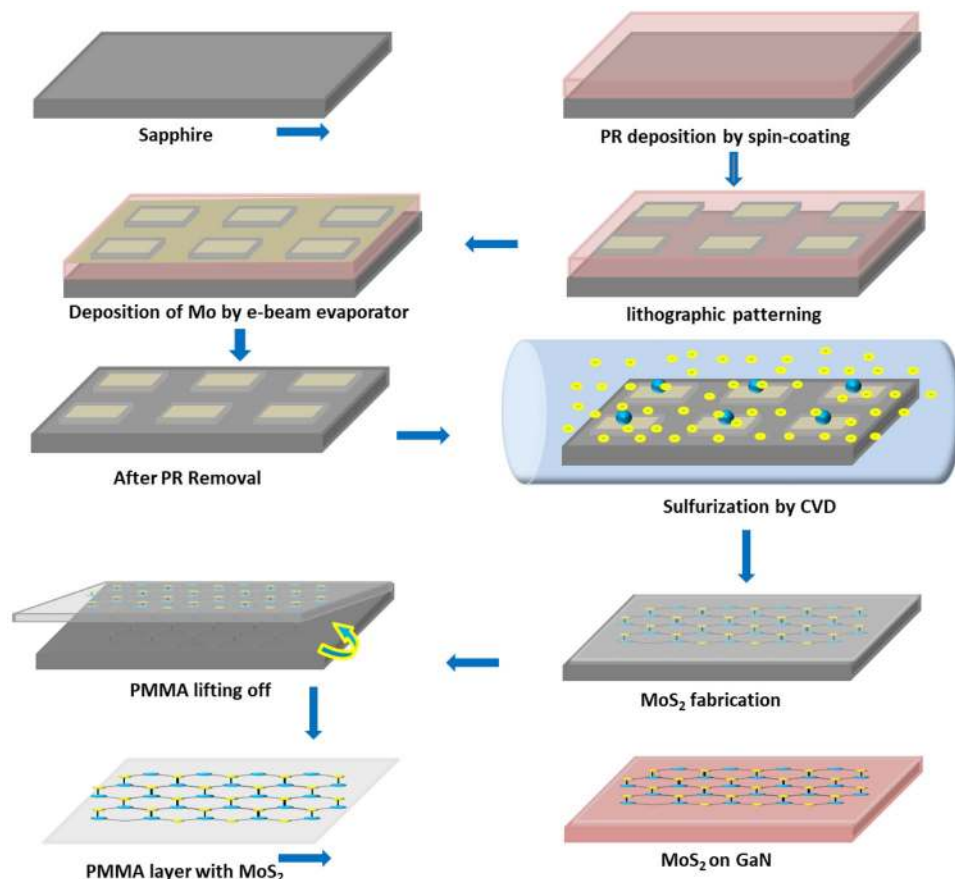


Figure 1. Schematic representation for the growth and transfer process of MoS₂ monolayer arrays onto a GaN substrate to fabricate a MoS₂/GaN heterostructure photoanode.

former corresponds to the opposite vibration of two sulfur atoms in regard to the molybdenum (Mo) atom in the basal plane (in-plane vibration mode), while the latter results from the vertical vibration of only sulfur (S) atoms in opposite directions (out-of-plane vibration mode), as illustrated in the insets of Fig. 2(c)⁴⁶. As is known, the frequency difference (Δu) between these two Raman modes is quite sensitive to the layer thickness, and can thus be used to detect the number of MoS₂ two dimensional layers^{47–49}. The E_{2g}^1 to A_g^1 peak position difference (Δu) in the Raman spectra shown in Fig. 2(c) is $\sim 20 \text{ m}^{-1}$ which can be considered as strong evidence for ML-MoS₂. The aforementioned results match with those found in previous studies^{45,50}. To investigate the optical properties of the prepared ML-MoS₂, room-temperature PL spectra were collected over a range of 600–700 nm using a 532-nm laser as an excitation source. Figure 2(d) depicts the PL spectra measured for the ML-MoS₂ grown on a sapphire substrate. A strong PL peak (radiative recombination of A excitons) centered at 660 nm without a shoulder peak at $\sim 610 \text{ nm}$ (optical transitions from B excitons) was observed. In ML-MoS₂, the excited electrons and holes recombine through direct band-to-band transition at the K-point in the Brillouin zone³⁷, leading to strong PL near 1.88 eV. The superior optical properties and the observation of a single peak (A excitonic emission) again represent strong evidence that the ML-MoS₂ synthesized here is undoubtedly of high quality. Moreover, X-ray diffraction were employed to confirm the high quality of the as-synthesized ML-MoS₂ (Supplementary Fig. S1).

The synthesized MoS₂ films exhibit a very good crystalline quality as indicated by the Raman and PL measurements (Fig. 2c,d). To further elucidate the crystalline structure, we characterized the ML-MoS₂ with a high-resolution transmission electron microscope (HRTEM). Figure 3(a) shows that the ML-MoS₂ are uniformly continuous cross an area of micrometers. Figure 3(b) shows a typical TEM image of the as-synthesized ML-MoS₂ that confirms uniformity with no defects such as cracks, which suggests a clean surface and high-quality for the produced ML-MoS₂, in support of the Raman and PL results. The HRTEM image displayed in Fig. 3(c), together with the corresponding selected area electron diffraction (SAED) pattern in Fig. 3(d), reveal that the ML-MoS₂ is a single crystal with a hexagonal lattice structure. A periodic honeycomb arrangement of the atoms with an inter-planar spacing of $\sim 0.32 \text{ nm}$ is observed in Fig. 3(c). Mo and S atoms can also be identified in TEM images. The yellow and blue points correspond to the Mo and S atoms in the hexagonal structure, respectively.

To investigate the PEC properties of the ML-MoS₂/GaN photoanode, a three-electrode home-made PEC cell was designed, as shown in Fig. 4(a). More details for the PEC measurements are provided in the Experimental section. MoS₂/GaN served as the working photoelectrode to absorb illuminated light energy and to convert it into electron-hole pairs, which then started the respective water splitting half reactions. Due to the conventional band bending of the semiconductors, the photogenerated electron-hole pairs will be separated, where the holes will

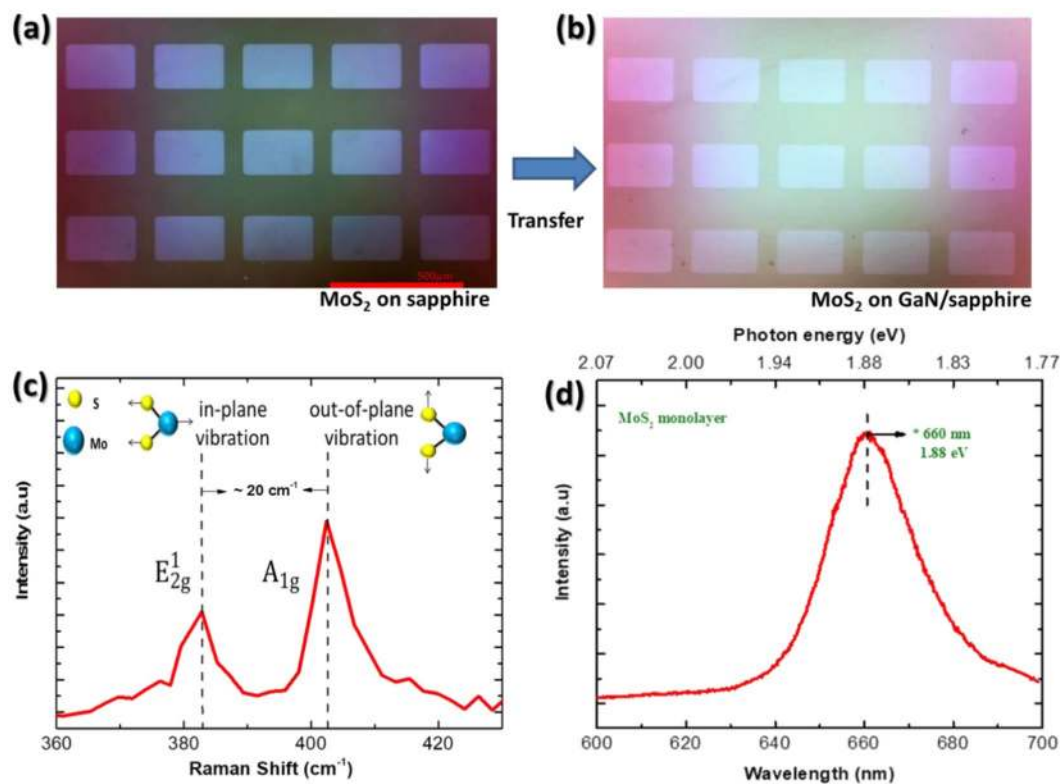


Figure 2. (a,b) Optical microscope images of a large continuous film of the synthesized monolayer MoS₂ with rectangular shaped patterns before and after the transfer process placed onto the sapphire and GaN substrates, respectively. (c) Typical Raman spectra for the monolayer MoS₂ grown on sapphire substrates. (d) Room-temperature PL spectra for the monolayer MoS₂ obtained using a 532-nm laser as an excitation source.

drift to the surface of the MoS₂/GaN to strip oxygen from the water (water oxidation) and the liberated electrons will migrate to the counter electrode (Pt wire) to convert hydrogen ions into molecular hydrogen gas (hydrogen reduction), as illustrated in Fig. 4(b).

To understand the basic PEC parameters for the fabricated photoelectrodes, we carried out in-depth electrochemical investigations for both GaN and MoS₂/GaN photoanodes using electrochemical impedance spectroscopy (EIS) under dark conditions. The EIS measurements were performed with the voltage amplitude of 20 mV for various frequencies (1.0 Hz–100 kHz). Figure 5(a,b) show the resulting Nyquist plots constructed from the electrochemical impedance spectra measured for GaN and MoS₂/GaN photoanodes, respectively. Semicircles can be clearly distinguished in the Nyquist plots for each sample, which were used to understand the charge transfer process at the electrode/electrolyte interface, with the semicircle diameter being equivalent to the charge transfer resistance⁵¹. The smaller diameter of the semicircle for the MoS₂/GaN electrode confirmed faster charge transfer process as well as more effective electron–hole pairs separation. Based on the results shown by Nyquist plots, we can conclude that the MoS₂ plays a significant role in increasing the light absorption, accelerating the charge separation and transfer at the interface, which enhances the PEC performance. As a result, the MoS₂/GaN heterostructure could be a potential photoanode for high-efficiency solar hydrogen generation because of fast charge separation and transport. To ensure that the MoS₂/GaN photoanode hasn't been degraded during the EIS measurement, a cyclic voltammetry (CV) scan is conducted before and after EIS measurement (Supplementary Fig. S2).

To gain further insights into the enhanced PEC performance of the MoS₂/GaN photoanodes, capacitance–potential relation was investigated in 1.0 M NaOH electrolyte under dark conditions over the potential range of –1.5 to 0.7 V vs Ag/AgCl electrode. The space-charge capacitance of the semiconductor and flat-band potential values which can be estimated from Mott–Schottky (MS) plots, were analyzed according to the MS equation shown in Eq. (1)⁵²

$$\frac{1}{C^2} = \frac{2}{\varepsilon\varepsilon_0eN_A} \left[(V - V_{fb}) - \frac{k_B T}{e} \right] \quad (1)$$

where C is the depletion capacitance of the semiconductor layer, V is the applied potential, V_{fb} is the flat-band potential, N_A is the acceptor concentration, e is the elemental charge value, ε₀ is permittivity of vacuum (ε₀ = 8.86 × 10⁻¹² Fm⁻¹), ε is the dielectric constant of the semiconductor, T is the absolute temperature, and k_B is the Boltzmann constant. The flat band potential can be obtained from the intercept of the plot tangents with the potential axis (C⁻² = 0). The positive slopes of the tangent lines in the MS plot display the n-type property for both

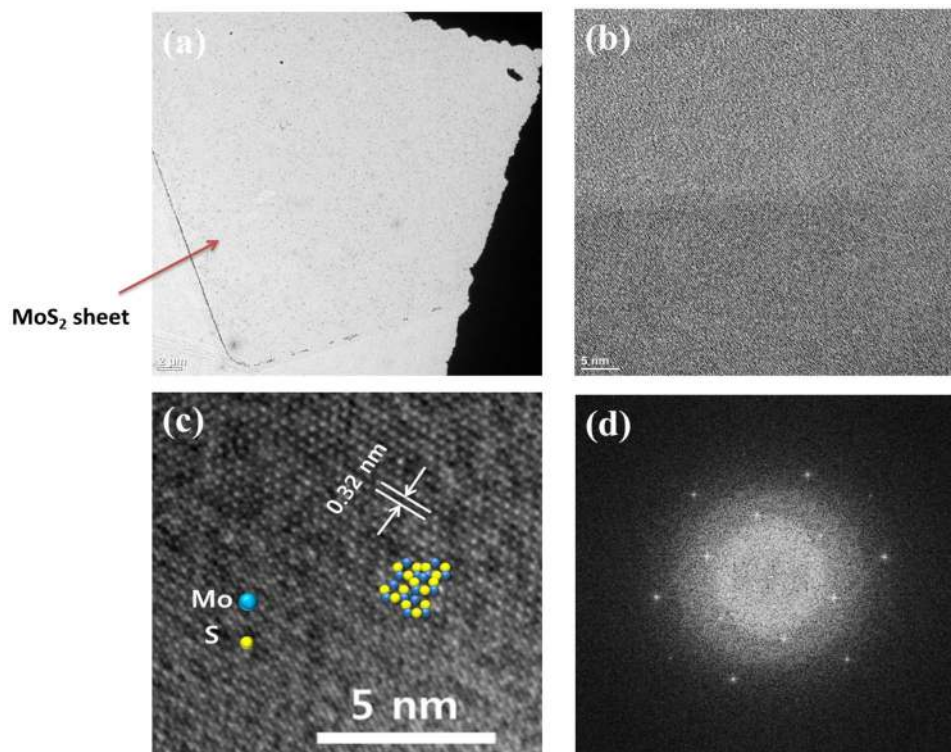


Figure 3. (a) Large-area uniformity for the synthesized MoS₂ monolayer. (b) Typical TEM image of the as synthesized monolayer MoS₂. (c) High-resolution TEM image of monolayer MoS₂. The insets show modeled crystal structures for the MoS₂ monolayer with the blue and yellow dots corresponding to Mo and S atoms, respectively. (d) SAED pattern for monolayer MoS₂ confirmed the hexagonal structured phase.

photoanodes, for which the lowest potential of the conduction band can be extremely close to its flat-band potential, as illustrated in Fig. 6(a,b). The flat-band potentials for the GaN and MoS₂/GaN photoanodes were calculated to be -0.88 V and -0.21 V vs Ag/AgCl, respectively.

The PEC performance of the MoS₂/GaN photoanode features light-driven water splitting process to investigate its potential as high-performance photoelectrodes. Linear sweeps voltammetry (LSV) were measured for pristine GaN and the MoS₂/GaN photoanodes at a sweep rate of 20 mV/s, as depicted in Fig. 7(a). The photocurrent densities were measured as a function of the applied bias between the as-synthesized working electrodes (pristine GaN and MoS₂/GaN) and the reference electrode, both in the dark and under illuminated conditions using 1 M NaOH as an electrolyte. Negligible dark currents were observed for all samples, revealing that the obtained photocurrent densities for all the prepared photoanodes are almost entirely generated through light irradiation. Compared to the pristine GaN, the MoS₂/GaN photoanode showed increased photocurrent in the anodic bias condition. At zero bias vs Ag/AgCl, the MoS₂/GaN photoanode exhibited a photocurrent density of 5.2 mA cm⁻², about 2.6 times higher than that of the reference GaN. The observed photocurrent density is mainly subjected to the improved carrier extraction/collection efficiency and the faster charge carrier transport to the desired water redox interfaces. CV measurements for pristine GaN and MoS₂/GaN photoanode including the Tafel plots obtained from CV curves have been conducted for further confirmation for the improved PEC properties (Supplementary Fig. S3). The superior water splitting behavior of the MoS₂/GaN photoanode can be partly ascribed to the enhanced solar absorption due to the introduction of MoS₂ as a cocatalyst with a narrow band gap (1.88 eV) that possesses the ability to absorb a significant portion of the entire solar spectrum, resulting in the generation of an increased number of electron-hole pairs^{37,38}. In contrast, GaN with its large band gap energy will limit the solar absorption to photon energies in the UV region, which represents a small portion of the solar spectrum, thereby resulting in a small photocurrent density when exposed to the simulated sunlight^{53,54}. The data in Fig. 7(b) shows the applied-bias-photon-to-current conversion efficiency (ABPE) to quantitatively evaluate the efficiency of the MoS₂/GaN photoanode with respect to the applied potential. The ABPE is given according to Eq. (2)⁵⁵

$$ABPE(\%) = 100 \times J(\text{mA cm}^{-2})(1.23 - V_{app})/P_{light}(\text{mW cm}^{-2}) \quad (2)$$

where J is the current density under visible light irradiation, 1.23 V is the standard-state reversible potential of water, V_{app} is the applied potential versus Ag/AgCl, and P_{light} is power density of light illumination. The applied potential was converted relative to the reversible hydrogen electrode (RHE). The conversion from Ag/AgCl to RHE is calculated using the Nernst equation: $E_{(RHE)} = E_{(Ag/AgCl)}^0 + E_{(Ag/AgCl)} + 0.059 \times pH$, where $E_{(RHE)}$ is the converted potential relative to RHE, $E_{(Ag/AgCl)}^0$ is the standard potential of the Ag/AgCl reference electrode, which

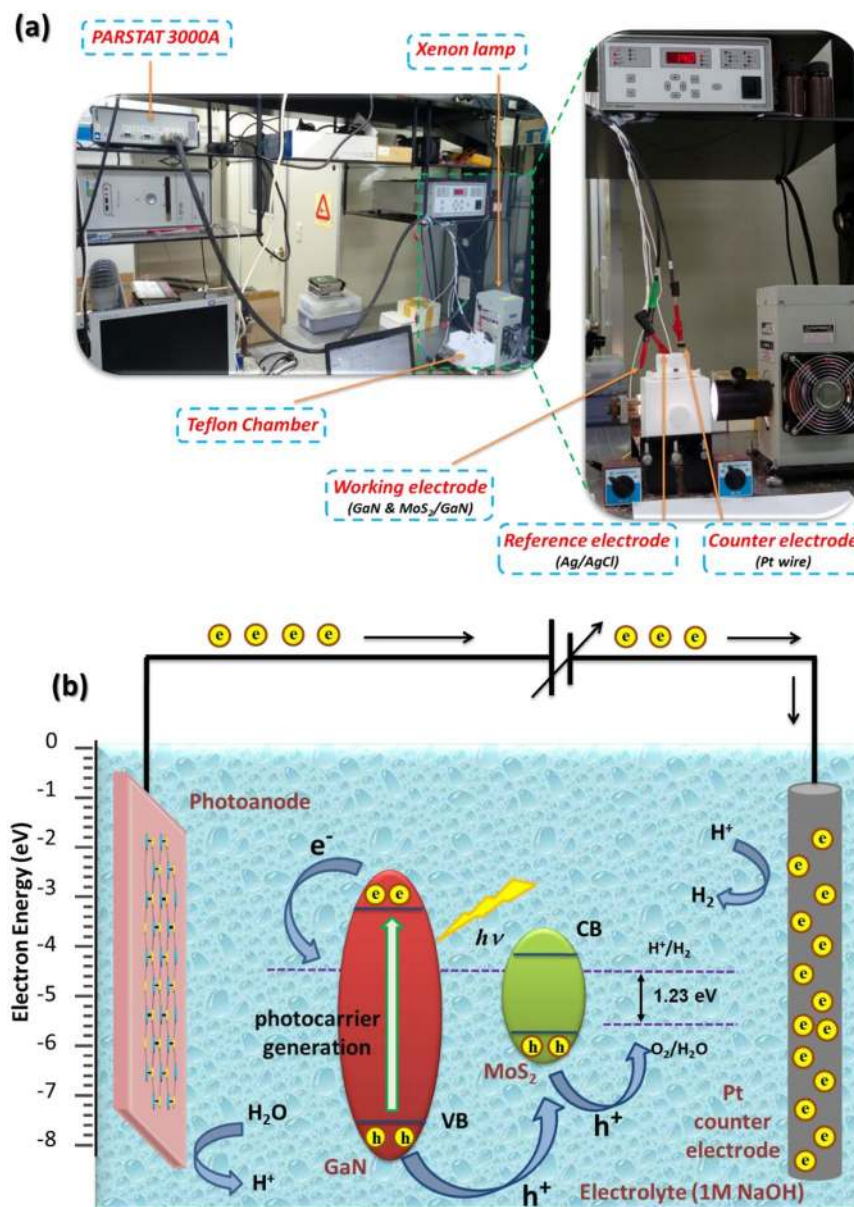


Figure 4. (a) Photographic images of the three-electrode home-made PEC cell used in the water splitting experiments. (b) Schematic diagram of the general PEC-WS process mechanism along with a band diagram for the MoS₂/GaN photoanode with respect to the water redox levels.

is equal (0.1976 V versus RHE at 25 °C), and $E_{(Ag/AgCl)}$ is the applied potential versus the Ag/AgCl reference electrode. The MoS₂/GaN photoanode achieved an ABPE of 0.91% at about 0.21 V vs. RHE. This result is a significant enhancement compared to only 0.32% at 0 V vs. RHE for the reference GaN. Thus, the efficiency of the power conversion was increased by almost 3 times by using MoS₂ as a cocatalyst coated onto GaN for the solar energy conversion device. To further investigate the photoresponse, long-term stability measurements were carried out using the chronoamperometry (CA) technique in 1 M NaOH under 500 mWcm⁻² irradiation, with an applied bias of 0 V vs. Ag/AgCl. Figure 7(c) displays the CA curves versus time plots measured for 45 min. The recorded photocurrent densities maintain consistency with the values obtained from the J-V curves, so the photocurrents are stable without giving rise to photoinduced charging effect. The slopes of the curves reflect the stabilities of the photoelectrodes; a smaller slope indicates better stability. The MoS₂/GaN photoanode exhibited a highly stable photocurrent density, approximately 5.2 mA cm⁻² at zero bias vs Ag/AgCl, which represents a 2.6-fold enhancement compared to that of reference GaN. Measurements under successive illumination for 45 min reveals no obvious decay in the photocurrent, which is substantially improved compared to the previous research focusing on GaN-based photoanodes. In addition, SEM was carried out for MoS₂/GaN after PEC stability measurements and showed that there is no degradation in the morphology (no corrosion) of the patterned ML MoS₂ (Supplementary Fig. S4(a-f)). As a result, the patterned ML MoS₂ inhibited the photocorrosion from the surface during the PEC experiments. X-ray photoelectron spectroscopy was performed after the stability test and it

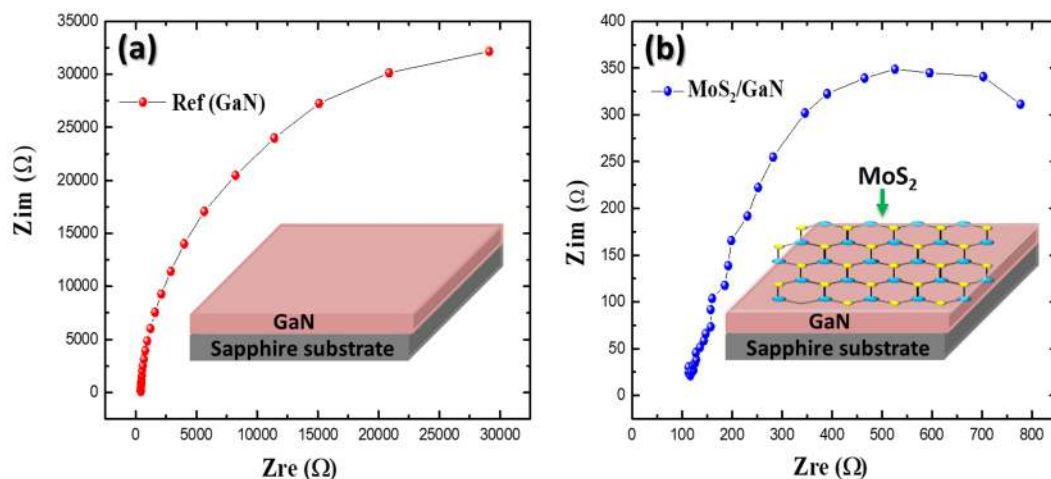


Figure 5. (a,b) Show the Nyquist plots for the GaN and MoS_2/GaN photoanodes, respectively.

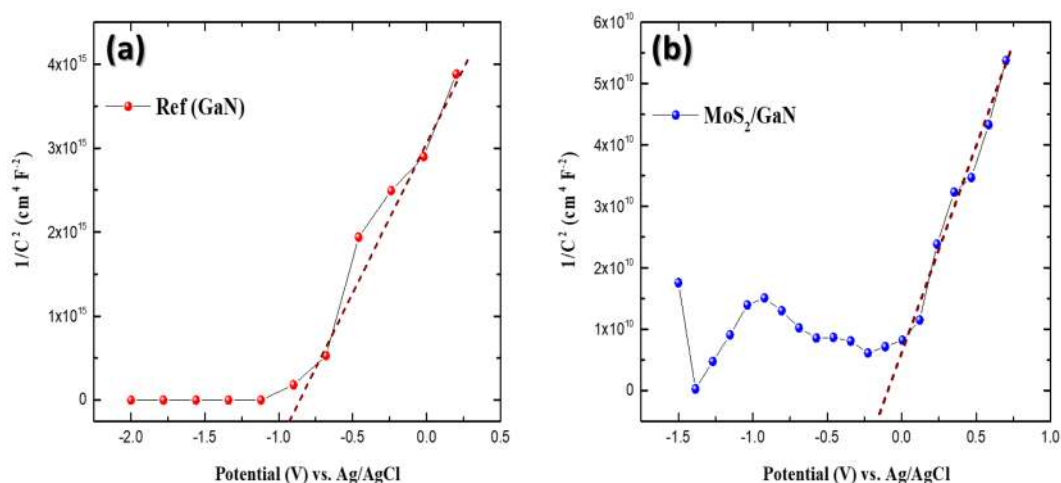


Figure 6. Mott–Schottky plots plotted as $1/C^2$ referenced to the Ag/AgCl electrode for (a) GaN and (b) MoS_2/GaN photoanodes.

showed clear signal from MoS_2 monolayer (Supplementary Fig. S5(a–f)). It is the evidence of stability of MoS_2 during the long-term water splitting process. Furthermore, no degradation of the electrode material is observed by monitoring the surface morphology using an optical microscope following the PEC water splitting experiment, which suggests that there may not be any structural or morphological changes in the electrodes. This study clearly demonstrates that the MoS_2 can significantly enhance the separation efficiency of photogenerated charge carriers in the MoS_2/GaN photoanode.

Conclusions

In summary, a facile strategy to synthesize a MoS_2/GaN heterostructure photoanode for solar water splitting and hydrogen fuel generation was proposed. First, single-crystalline GaN was grown onto a c-plane sapphire substrate by MOCVD. Then, MoS_2 was subsequently deposited by a Mo-sulfurization technique before being transferred onto GaN to form a MoS_2/GaN heterojunction. The synthesized samples were analyzed in detail by TEM, PL, and Raman, and the fabrication of high-quality ML- MoS_2 was confirmed. The resulting MoS_2/GaN photoanode exhibited excellent PEC performance, including a photocurrent value of 5.2 mA cm^{-2} and a high photo-to-hydrogen conversion efficiency of 0.91%, which indicates great improvements in performance compared to pristine GaN. The significant enhancement in photocurrent density and efficiency that were observed can be attributed to the visible response of the MoS_2 layer, which reduced the charge transfer resistance between the semiconductor and the electrolyte interface and the improvement of the charge separation in the MoS_2/GaN heterostructure. This work demonstrates potential advantages of the MoS_2/GaN heterostructure photoanode for PEC water splitting and provides an important methodology for the fabrication and design of III–V semiconductor surfaces with two-dimensional co-catalyst materials for solar-driven hydrogen production.

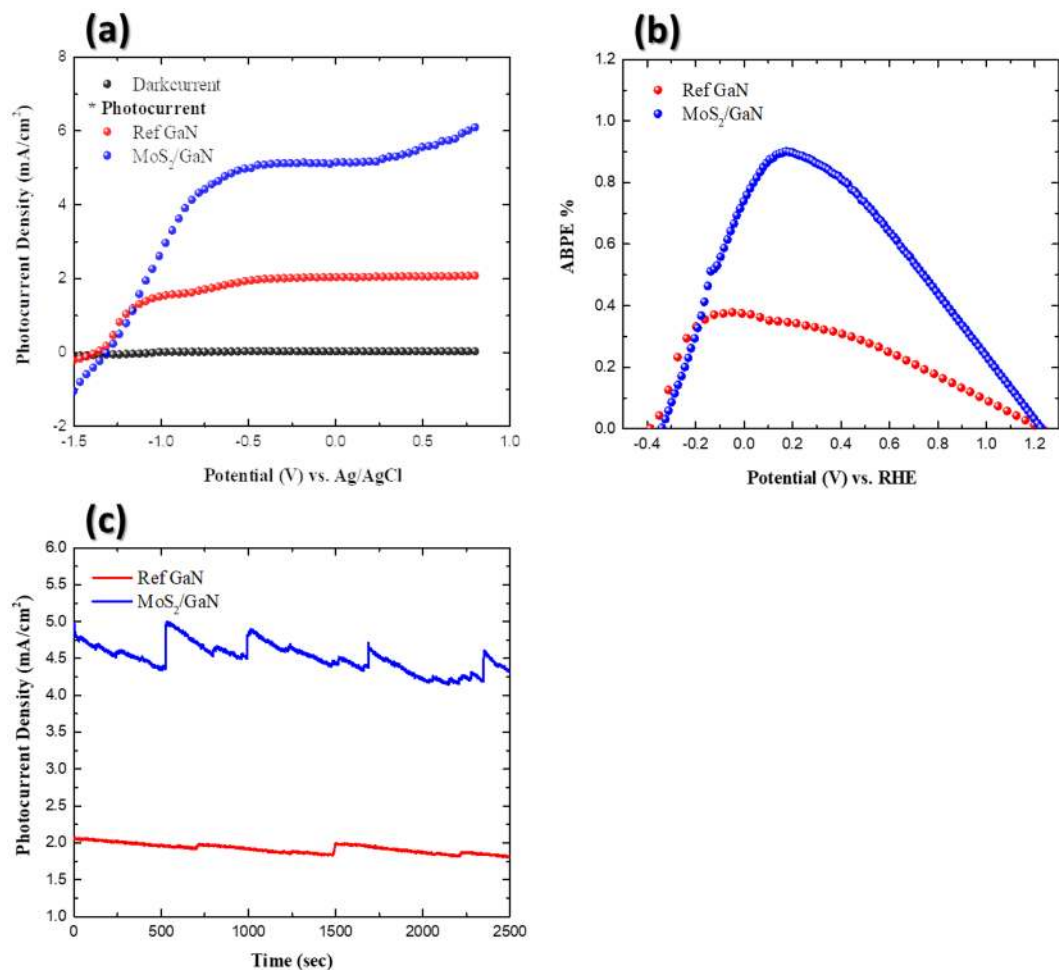


Figure 7. PEC performance of the MoS₂/GaN photoanode as compared to GaN (a) LSV for the MoS₂/GaN photoanode as a function of the applied potential referenced to the Ag/AgCl electrode. The data were obtained in the dark and under light illumination. (b) ABPE of the MoS₂/GaN photoanode as a function of the applied potential referenced to RHE. (c) Chronoamperometric test of the MoS₂/GaN photoanode as a function of working time measured at 0 V.

Methods

Synthesis of GaN on a c-plane sapphire substrate. Sample fabrication started with the growth of undoped GaN on a c-plane sapphire substrate by metal-organic chemical vapor deposition (MOCVD). Trimethylgallium (TMGa) and NH₃ were used as precursors for gallium and nitrogen, respectively. To reduce the stress in the GaN thin film due to the lattice mismatch between GaN and sapphire, a very thin buffer layer of GaN was grown at low temperature of 600 °C. Then, the temperature of the reactor was increased up to 1175 °C for 2.5 μm-thick GaN. The flow rates of TMGa and NH₃ were 292.67 μmol/min and 401.78 mmol/min, respectively, corresponding to a V/III ratio of 1372.9. The growth was performed for 3500 s at the reactor pressure of 100 torr while H₂ was used as the main carrier gas.

Synthesis of MoS₂ on GaN. After lithographic patterning of the photoresist layer, a 1-nm-thick thin film of Mo was deposited onto a sapphire substrate by e-beam evaporation. The process began with the patterning of a Mo film array with rectangular windows (110 × 190 μm²) by photolithography. Next, patterned Mo thin films deposited on sapphire substrates were placed in a quartz boat, which was in turn placed in the center of a chemical vapor deposition (CVD) tube furnace. A ceramic boat containing pure sulfur (>99.99%, 0.8 g, Sigma-Aldrich) was placed in the upwind low-temperature zone in the quartz tube. During the reaction, the temperature in the low temperature zone was controlled to be just above the melting point of sulfur (113 °C). The quartz tube was first held under Ar at a flow rate of 100 sccm. The temperature was raised from room temperature to 750 °C at a ramp up rate of 75 °C min⁻¹, and then held constant for 5 min before being naturally cooled down to room temperature in 60 min. To study solar-driven water splitting, CVD-grown single domains of MoS₂ were transferred (using PMMA as a support film and 5 M NaOH/NaF solution) onto a GaN epilayer grown onto a sapphire substrate by MOCVD. The PMMA film was dissolved in acetone and the residue removed by annealing in Ar at 150 °C for 30 min.

Material characterizations. The nanostructure and crystal quality of single domains of MoS₂ were characterized by using high-resolution TEM with the atomic resolution, operating at 200 keV. Raman spectra for the MoS₂ nanosheets were obtained by using a 532-nm laser excitation source operating at 6 mW. The room temperature PL for MoS₂ was measured using a 532-nm laser with optical power of approximately 6 mW.

PEC water splitting experiments. PEC experiments were performed in a three-electrode home-made cell wired to a typical potentiostat/galvanostat (Parstat 3000 A, Princeton Applied Research), operated by VersaStudio software. The as-synthesized samples were mounted onto a Teflon chamber cell having a size of $16 \times 9 \times 10 \text{ cm}^3$ ($L \times W \times H$). The MoS₂/GaN photoanode, a Pt wire, and an Ag/AgCl electrode (sodium-chloride-saturated silver chloride electrode) were used as the working, counter, and reference electrodes, respectively. 1 M NaOH aqueous solution was used as the electrolyte. The MoS₂/GaN photoanode was mounted onto the Teflon chamber, where the sample surface was directly in contact with the electrolyte through a hole with a diameter of approximately 0.5 cm. Then a conductive Cu wire was bonded to the MoS₂/GaN photoanode surface using indium contact and wired to the counter electrode for hole transport. The sample was irradiated through a transparent quartz window using simulated sunlight provided by a 300 W Xe lamp (Newport 66902). The light irradiance was kept constant at 500 mW cm^{-2} during the measurements and illuminated surface area was about 0.5026 cm^2 . The chronoamperometry and linear scan voltammetry (LSV) (scan rate of 20 mV/s) experiments were performed using the single channel potentiostat. The performance of the MoS₂/GaN photoanode was assessed based on the photocurrent density–voltage (J – V) curves evaluated both in the dark and under illumination.

Received: 13 April 2019; Accepted: 15 November 2019;

Published online: 27 December 2019

References

- Zou, Z., Ye, J., Sayama, K. & Arakawa, H. Direct splitting of water under visible light irradiation with an oxide semiconductor photocatalyst. *Nature* **414**, 625 (2001).
- Davis, S. J., Caldeira, K. & Matthews, H. D. Future CO₂ Emissions and Climate Change from Existing Energy Infrastructure. *Science* **329**, 1330–1333 (2010).
- Dresselhaus, M. S. & Thomas, I. L. Alternative energy technologies. *Nature* **414**, 332 (2001).
- Grätzel, M. Photoelectrochemical cells. *Nature* **414**, 338 (2001).
- Chen, X., Shen, S., Guo, L. & Mao, S. S. Semiconductor-based Photocatalytic Hydrogen Generation. *Chem. Rev.* **110**, 6503–6570 (2010).
- Paracchino, A., Laporte, V., Sivula, K., Grätzel, M. & Thimsen, E. Highly active oxide photocathode for photoelectrochemical water reduction. *Nature Materials* **10**, 456–461 (2011).
- Fujishima, A. & Honda, K. Electrochemical Photolysis of Water at a Semiconductor Electrode. *Nature* **238**, 37 (1972).
- Wang, D. *et al.* Crystallinity Engineering of Hematite Nanorods for High-Efficiency Photoelectrochemical Water Splitting. *Adv. Sci. (Weinh)* **2** (2015).
- Wang, Y. *et al.* Bio-Inspired Leaf-Mimicking Nanosheet/Nanotube Heterostructure as a Highly Efficient Oxygen Evolution Catalyst. *Adv. Sci. (Weinh)* **2**, 1500003 (2015).
- Li, Z., Yao, C., Yu, Y., Cai, Z. & Wang, X. Highly Efficient Capillary Photoelectrochemical Water Splitting Using Cellulose Nanofiber-Templated TiO₂ Photoanodes. *Advanced Materials* **26**, 2262–2267 (2014).
- Bak, T., Nowotny, J., Rekas, M. & Sorrell, C. C. Photo-electrochemical hydrogen generation from water using solar energy. Materials-related aspects. *International Journal of Hydrogen Energy* **27**, 991–1022 (2002).
- Warren, E. L., McKone, J. R., Atwater, H. A., Gray, H. B. & Lewis, N. S. Hydrogen-evolution characteristics of Ni–Mo-coated, radial junction, n+p-silicon microwire array photocathodes. *Energy Environ. Sci.* **5**, 9653–9661 (2012).
- Smith, Y. R., Sarma, B., Mohanty, S. K. & Misra, M. Single-step anodization for synthesis of hierarchical TiO₂ nanotube arrays on foil and wire substrate for enhanced photoelectrochemical water splitting. *International Journal of Hydrogen Energy* **38**, 2062–2069 (2013).
- Deshmukh, P. R., Sohn, Y. & Shin, W. G. Chemical synthesis of ZnO nanorods: Investigations of electrochemical performance and photo-electrochemical water splitting applications. *Journal of Alloys and Compounds* **711**, 573–580 (2017).
- Monfort, O. *et al.* Photoelectrocatalytic hydrogen production by water splitting using BiVO₄ photoanodes. *Chemical Engineering Journal* **286**, 91–97 (2016).
- Qiu, Y. *et al.* Efficient photoelectrochemical water splitting with ultrathin films of hematite on three-dimensional nanophotonic structures. *Nano Lett.* **14**, 2123–2129 (2014).
- Ho, G. W., Chua, K. J. & Siow, D. R. Metal loaded WO₃ particles for comparative studies of photocatalysis and electrolysis solar hydrogen production. *Chemical Engineering Journal* **181–182**, 661–666 (2012).
- Kudo, A. Recent progress in the development of visible light-driven powdered photocatalysts for water splitting. *International Journal of Hydrogen Energy* **32**, 2673–2678 (2007).
- Hassan, M. A., Kang, J.-H., Johar, M. A., Ha, J.-S. & Ryu, S.-W. High-performance ZnS/GaN heterostructure photoanode for photoelectrochemical water splitting applications. *Acta Materialia* **146**, 171–175 (2018).
- Kudo, A. & Miseki, Y. Heterogeneous photocatalyst materials for water splitting. *Chem. Soc. Rev.* **38**, 253–278 (2009).
- Su, J., Guo, L., Bao, N. & Grimes, C. A. Nanostructured WO₃/BiVO₄ Heterojunction Films for Efficient Photoelectrochemical Water Splitting. *Nano Lett.* **11**, 1928–1933 (2011).
- Walter, M. G. *et al.* Solar Water Splitting Cells. *Chem. Rev.* **110**, 6446–6473 (2010).
- Fan, S. *et al.* High Efficiency Solar-to-Hydrogen Conversion on a Monolithically Integrated InGaN/GaN/Si Adaptive Tunnel Junction Photocathode. *Nano Lett.* **15**, 2721–2726 (2015).
- AlOtaibi, B., Fan, S., Vanka, S., Kibria, M. G. & Mi, Z. A Metal-Nitride Nanowire Dual-Photoelectrode Device for Unassisted Solar-to-Hydrogen Conversion under Parallel Illumination. *Nano Lett.* **15**, 6821–6828 (2015).
- Aryal, K., Pantha, B. N., Li, J., Lin, J. Y. & Jiang, H. X. Hydrogen generation by solar water splitting using p-InGaN photoelectrochemical cells. *Appl. Phys. Lett.* **96**, 052110 (2010).
- Waki, I. *et al.* Direct water photoelectrolysis with patterned n-GaN. *Appl. Phys. Lett.* **91**, 093519 (2007).
- Yu, Y., Zhang, J., Wu, X., Zhao, W. & Zhang, B. Nanoporous Single-Crystal-Like Cd_xZn_{1-x}S Nanosheets Fabricated by the Cation-Exchange Reaction of Inorganic–Organic Hybrid ZnS–Amine with Cadmium Ions. *Angewandte Chemie International Edition* **51**, 897–900 (2012).
- Kim, S. H., Kang, J.-H. & Ryu, S.-W. Enhanced water splitting stability with controlled NiO co-catalyst on GaN photoanode. *J. Nanosci. Nanotechnol.* **14**, 7903–7906 (2014).

29. Kim, S. H., Ebaid, M., Kang, J.-H. & Ryu, S.-W. Improved efficiency and stability of GaN photoanode in photoelectrochemical water splitting by NiO cocatalyst. *Applied Surface Science* **305**, 638–641.
30. Huang, X., Zeng, Z. & Zhang, H. Metal dichalcogenide nanosheets: preparation, properties and applications. *Chem. Soc. Rev.* **42**, 1934–1946 (2013).
31. Wang, Q. H., Kalantar-Zadeh, K., Kis, A., Coleman, J. N. & Strano, M. S. Electronics and optoelectronics of two-dimensional transition metal dichalcogenides. *Nature Nanotechnology* **7**, 699–712 (2012).
32. Jariwala, D., Sangwan, V. K., Lauhon, L. J., Marks, T. J. & Hersam, M. C. Emerging device applications for semiconducting two-dimensional transition metal dichalcogenides. *ACS Nano* **8**, 1102–1120 (2014).
33. Lu, Q., Yu, Y., Ma, Q., Chen, B. & Zhang, H. 2D Transition-Metal-Dichalcogenide-Nanosheet-Based Composites for Photocatalytic and Electrocatalytic Hydrogen Evolution Reactions. *Adv. Mater. Weinheim* **28**, 1917–1933 (2016).
34. Zhang, J. *et al.* Crystal face regulating MoS₂/TiO₂(001) heterostructure for high photocatalytic activity. *Journal of Alloys and Compounds* **688**, 840–848 (2016).
35. Hao, L. *et al.* Electrical and photovoltaic characteristics of MoS₂/Si p-n junctions. *Journal of Applied Physics* **117**, 114502 (2015).
36. Coleman, J. N. *et al.* Two-Dimensional Nanosheets Produced by Liquid Exfoliation of Layered. *Materials. Science* **331**, 568–571 (2011).
37. Mak, K. F., Lee, C., Hone, J., Shan, J. & Heinz, T. F. Atomically thin MoS₂: A new direct-gap semiconductor. *Physical Review Letters* **105**, 136805 (2010).
38. Splendiani, A. *et al.* Emerging Photoluminescence in Monolayer MoS₂. *Nano Lett.* **10**, 1271–1275 (2010).
39. Maitra, U. *et al.* Highly Effective Visible-Light-Induced H₂ Generation by Single-Layer 1T-MoS₂ and a Nanocomposite of Few-Layer 2H-MoS₂ with Heavily Nitrogenated Graphene. *Angewandte Chemie International Edition* **52**, 13057–13061 (2013).
40. Hinnemann, B. *et al.* Biomimetic Hydrogen Evolution: MoS₂ Nanoparticles as Catalyst for Hydrogen Evolution. *J. Am. Chem. Soc.* **127**, 5308–5309 (2005).
41. Jaramillo, T. F. *et al.* Identification of Active Edge Sites for Electrochemical H₂ Evolution from MoS₂ Nanocatalysts. *Science* **317**, 100–102 (2007).
42. Awasthi, G. P. *et al.* Facile synthesis of ZnO flowers modified graphene like MoS₂ sheets for enhanced visible-light-driven photocatalytic activity and antibacterial properties. *Journal of Alloys and Compounds* **682**, 208–215 (2016).
43. Yuan, Y.-J. *et al.* Constructing Anatase TiO₂ Nanosheets with Exposed (001) Facets/Layered MoS₂ Two-Dimensional Nanojunctions for Enhanced Solar Hydrogen Generation. *ACS Catal.* **6**, 532–541 (2016).
44. Li, H. *et al.* From Bulk to Monolayer MoS₂: Evolution of Raman Scattering. *Advanced Functional Materials* **22**, 1385–1390 (2012).
45. Lee, C. *et al.* Anomalous Lattice Vibrations of Single- and Few-Layer MoS₂. *ACS Nano* **4**, 2695–2700 (2010).
46. Sun, L. *et al.* Plasma Modified MoS₂ Nanoflakes for Surface Enhanced Raman Scattering. *Small* **10**, 1090–1095 (2014).
47. Zhan, Y., Liu, Z., Najmaei, S., Ajayan, P. M. & Lou, J. Large-Area Vapor-Phase Growth and Characterization of MoS₂ Atomic Layers on a SiO₂ Substrate. *Small* **8**, 966–971 (2012).
48. Yu, Y. *et al.* Controlled Scalable Synthesis of Uniform, High-Quality Monolayer and Few-layer MoS₂ Films. *Scientific Reports* **3**, 1866 (2013).
49. Plechinger, G. *et al.* Raman spectroscopy of the interlayer shear mode in few-layer MoS₂ flakes. *Appl. Phys. Lett.* **101**, 101906 (2012).
50. Najmaei, S. *et al.* Vapour phase growth and grain boundary structure of molybdenum disulphide atomic layers. *Nature Materials* **12**, 754–759 (2013).
51. Zhang, Z. & Wang, P. Highly stable copper oxide composite as an effective photocathode for water splitting via a facile electrochemical synthesis strategy. *J. Mater. Chem.* **22**, 2456–2464 (2012).
52. Zhang, Z. & Wang, P. Optimization of photoelectrochemical water splitting performance on hierarchical TiO₂ nanotube arrays. *Energy Environ. Sci.* **5**, 6506–6512 (2012).
53. AlOtaibi, B. *et al.* Highly Stable Photoelectrochemical Water Splitting and Hydrogen Generation Using a Double-Band InGaN/GaN Core/Shell Nanowire Photoanode. *Nano. Lett.* **13**, 4356–4361 (2013).
54. Li, J., Lin, J. Y. & Jiang, H. X. Direct hydrogen gas generation by using InGaN epilayers as working electrodes. *Appl. Phys. Lett.* **93**, 162107 (2008).
55. Ebaid, M. *et al.* Unbiased photocatalytic hydrogen generation from pure water on stable Ir-treated In_{0.33}Ga_{0.67}N nanorods. *Nano. Energy* **37**, 158–167 (2017).

Acknowledgements

This work was supported by Priority Research Centers Program through the National Research Foundation of Korea (NRF) funded by the Ministry of Education, Science and Technology(2018R1A6A1A03024334) and by the National Research Foundation of Korea Grant funded by the Korean Government (NRF-2019R1A2C1006360).

Author contributions

M.A. Hassan and S.-W. Ryu designed the research, analyzed data and wrote the paper. M.-W. Kim and M.-K. Kwon developed MoS₂ fabrication technique. M.A. Johar and A. Waseem contributed extensively to the growth of GaN on sapphire substrate. All authors reviewed the manuscript.

Competing interests

The authors declare no competing interests.

Additional information

Supplementary information is available for this paper at <https://doi.org/10.1038/s41598-019-56807-y>.

Correspondence and requests for materials should be addressed to S.-W.R.

Reprints and permissions information is available at www.nature.com/reprints.

Publisher's note Springer Nature remains neutral with regard to jurisdictional claims in published maps and institutional affiliations.



Open Access This article is licensed under a Creative Commons Attribution 4.0 International License, which permits use, sharing, adaptation, distribution and reproduction in any medium or format, as long as you give appropriate credit to the original author(s) and the source, provide a link to the Creative Commons license, and indicate if changes were made. The images or other third party material in this article are included in the article's Creative Commons license, unless indicated otherwise in a credit line to the material. If material is not included in the article's Creative Commons license and your intended use is not permitted by statutory regulation or exceeds the permitted use, you will need to obtain permission directly from the copyright holder. To view a copy of this license, visit <http://creativecommons.org/licenses/by/4.0/>.

© The Author(s) 2019